The Resolved Asteroid Program - Size, shape, and pole of (52) Europa[☆]

W. J. Merline[a], J. D. Drummond[b], B. Carry[c,d], A. Conrad[e,f], P. M. Tamblyn[a], C. Dumas[g], M. Kaasalainen[h], A. Erikson[i], S. Mottola[i], J. Ďurech[j], G. Rousseau[k], R. Behrend[k,l], G. B. Casalnuovo[k,m], B. Chinaglia[k,m], J. C. Christou[n], C. R. Chapman[a], C. Neyman[f]

[a]*Southwest Research Institute, 1050 Walnut St. # 300, Boulder, CO 80302, USA*
[b]*Starfire Optical Range, Directed Energy Directorate, Air Force Research Laboratory, Kirtland AFB, NM 87117-577, USA*
[c]*IMCCE, Observatoire de Paris, CNRS, 77 av. Denfert Rochereau, 75014 Paris, France*
[d]*European Space Astronomy Centre, ESA, P.O. Box 78, 28691 Villanueva de la Cañada, Madrid, Spain*
[e]*Max-Planck-Institut für Astronomie, Königstuhl, 17, Heidelberg, Germany*
[f]*W.M. Keck Observatory, 65-1120 Mamalahoa Highway, Kamuela, HI 96743, USA*
[g]*ESO, Alonso de Córdova 3107, Vitacura, Casilla 19001, Santiago de Chile, Chile*
[h]*Tampere University of Technology, P.O. Box 553, 33101 Tampere, Finland*
[i]*Institute of Planetary Research, DLR, Rutherfordstrasse 2, 12489, Berlin, Germany*
[j]*Astronomical Institute, Faculty of Mathematics and Physics, Charles University in Prague, V Holešovičkách 2, 18000 Prague, Czech Republic*
[k]*CdR & CdL group: Lightcurves of minor planets and variable stars*
[l]*Geneva Observatory, 1290 Sauverny, Switzerland*
[m]*Eurac Observatory, Bolzano*
[n]*Gemini Observatory, 670 N. Aohoku Place, Hilo, Hawaii, 96720, USA*

arXiv:1301.5101v1 [astro-ph.EP] 22 Jan 2013

Abstract

With the adaptive optics (AO) system on the 10 m Keck-II telescope, we acquired a high quality set of 84 images at 14 epochs of asteroid (52) Europa on 2005 January 20, when it was near opposition. The epochs covered its 5.63 h rotation period and, by following its changing shape and orientation on the plane of sky, we obtained its triaxial ellipsoid dimensions and spin pole location. An independent determination from images at three epochs obtained in 2007 is in good agreement with these results. By combining these two data sets, along with a single epoch data set obtained in 2003, we have derived a global fit for (52) Europa of diameters $a \times b \times c = (379 \times 330 \times 249) \pm (16 \times 8 \times 10)$ km, yielding a volume-equivalent spherical-diameter of $\sqrt[3]{abc} = 315 \pm 7$ km, and a prograde rotational pole within 7° of [RA; Dec] = [257°; +12°] in an Equatorial J2000 reference frame (Ecliptic: 255°; +35°). Using the average of all mass determinations available for (52) Europa, we derive a density of 1.5 ± 0.4 g cm^{-3}, typical of C-type asteroids. Comparing our images with the shape model of Michalowski et al. (Astron. and Astrophys. 416, p 353, 2004), derived from optical lightcurves, illustrates excellent agreement, although several edge features visible in the images are not rendered by the model. We therefore derived a complete 3-D description of (52) Europa's shape using the KOALA algorithm by combining our 18 AO imaging epochs with 4 stellar occultations and 49 lightcurves. We use this 3-D shape model to assess these departures from ellipsoidal shape. Flat facets (possible giant craters) appear to be less distinct on (52) Europa than on other C-types that have been imaged in detail, (253) Mathilde and (511) Davida. We show that fewer giant craters, or smaller craters, is consistent with its expected impact history. Overall, asteroid (52) Europa is still well modeled as a smooth triaxial ellipsoid with dimensions constrained by observations obtained over several apparitions.

Keywords:

1. Introduction

Direct, accurate measurements of asteroid shapes, sizes, and pole positions are now possible for larger asteroids that can be spatially resolved using the Hubble Space Telescope (HST) or large ground-based telescopes equipped with adaptive optics (AO). Physical and statistical study of asteroids requires accurate knowledge of these parameters. Improved sizes permit improved estimates of albedo, in turn allowing better interpretation of surface composition. In those cases where we have an estimate of the mass, for example from the presence of a satellite, the uncertainty in the volume of the asteroid is the overwhelming uncertainty in attempts to derive its density (Merline et al. 2002). Of course, density is the single most critical observable having a bearing on bulk composition, porosity, and internal structure (Merline et al. 2002; Britt et al. 2002, 2006). With our technique of determining the size of an asteroid by following its changing apparent size, shape, and orientation, the uncertainties in volume can now be reduced to the level of the mass uncertainty, vastly improving our

[☆]Based on observations at the W. M. Keck Observatory, which is operated as a scientific partnership among the California Institute of Technology, the University of California and the National Aeronautics and Space Administration. The Observatory was made possible by the generous financial support of the W. M. Keck Foundation.

Email address: merline@boulder.swri.edu (W. J. Merline)

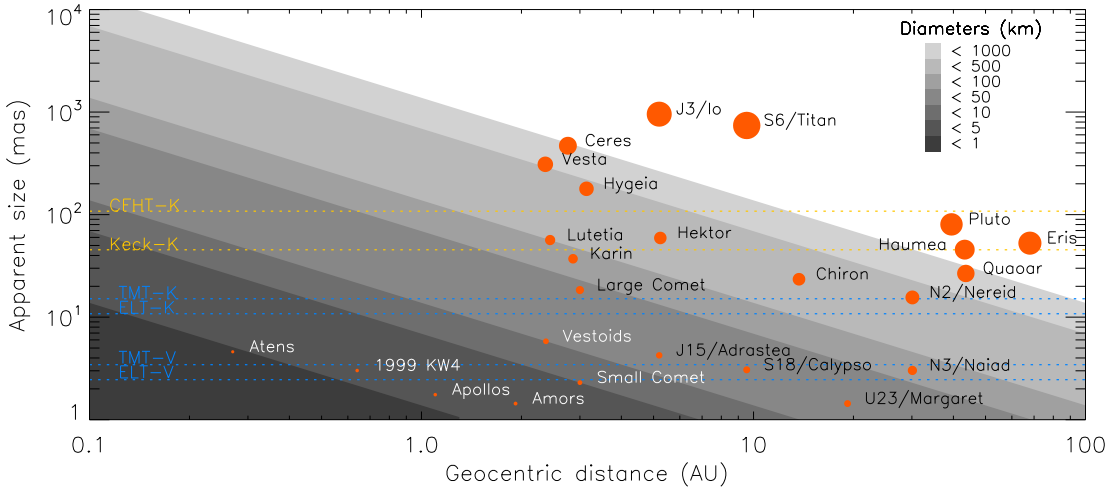


Figure 1: Apparent angular sizes of Solar System objects. Asteroid, moon, comet, and TNO diameters are plotted against their geocentric distances, defined as the difference between their semi-major axis and 1 AU. Symbol size corresponds to physical diameter. Gray scales represent the changing apparent size with geocentric distance. A body of a given size moves along the oblique lines as its distance from the Earth changes. The angular resolutions at CFHT, Keck and future TMT and E-ELT are also shown for different filters (V: 0.6 μm, and K: 2.2 μm). Typical NEA populations (Apollos, Atens, and Amors) are also shown, as represented by (1566) Icarus, (99942) Apophis, and (433) Eros, respectively.

confidence in the derived asteroid densities. The improvement comes about because we can see the detailed shape, track edge or surface features during rotation, and often can make an immediate pole determination.

Dedicated study of asteroids now allows directly observable shape profiles, and already has shown that some asteroids show large departures from a reference ellipsoid that may provide clues to the body's response to large impacts over time (*e.g.*, (4) Vesta, Thomas et al. 1997). For asteroid (511) Davida, we suggested (Conrad et al. 2007) that such features (*e.g.*, large flat facets) may be analogs of the giant craters, seen edge-on, in the images of (253) Mathilde during the NEAR mission (Veverka et al. 1999) flyby. If giant craters are evident on these surfaces, they can be related to the impact history and impact flux over time, and there is some chance they can be associated with asteroid families or clusters that are being identified by numerical back-integration and clustering of orbital elements (*e.g.*, Nesvorný et al. 2002).

As we have demonstrated with asteroid (511) Davida (Conrad et al. 2007), we can derive an asteroid's triaxial ellipsoid dimensions and rotational pole location in a single night. However, we now have developed the ability to combine sets of similar observations obtained at different viewing aspects to make a global fit to all of the images, drastically reducing dimension uncertainties that might be due to sparse rotational sampling or peculiar observing geometries (Drummond et al., in preparation). The leverage of widely spaced observations and the accompanying range of viewing aspects allows unprecedented accuracy in derived parameters. We can then use these estimates to project the apparent size and shape of an asteroid into the past or future, making the asteroid useful as a reference or calibration object.

Here we report on the physical properties of the asteroid (52) Europa as a part of our on-going *Resolved Asteroid Program*. We routinely image the apparent disk of asteroids, and search their close vicinity for companions, aiming at setting better constraints on their spin-vector coordinates, 3-D shapes, sizes, and multiplicity. One of our main goals is to derive (or better constrain) their densities. We use two independent methods to determine size, shape, and pole position of the target asteroids. One of these is based on the assumption that the shape is well-described by a smooth triaxial ellipsoid (see Drummond 2000; Drummond et al. 2009a, 2010, for instance). Our other method allows construction of full 3-D shape models by combining our AO images with other data types, when available (*e.g.*, optical lightcurves and stellar occultations, see Carry et al. 2010a,b), in the technique we call KOALA (Knitted Occultation, Adaptive-optics and Lightcurve Analysis, see Carry et al. 2010a; Kaasalainen 2011).

The best angular resolution, approximated by $\theta = \lambda/\mathcal{D}$ (radian), with λ the wavelength and $\mathcal{D}$ the diameter of the telescope aperture, of current ground-based optical telescopes is about 0.04″ (Keck/NIR). Due to systematics, however, we have found that our ability to accurately measure sizes and details of the apparent shape degrades below about 0.10″, based on simulations and observations of the moons of Saturn and simulations (Carry 2009; Drummond et al. 2009b). The sample of observable asteroids (*i.e.*, having angular sizes that get above about 0.10″) is therefore limited to about 200.

This limit in angular resolution can be converted to a physical diameter. As can be seen in Fig. 1, we can probe the size distribution of main-belt asteroids down to about 100 km, while Pluto is the only Trans-Neptunian Object (TNO) whose apparent disk can be resolved. At opportune times, we have been able to resolve the disks of Near-Earth Asteroids (NEAs, for example, see Merline et al. 2011, 2012). The next generation of optical facilities will allow an improvement in angular resolution by a factor of 3-4 due to mirror size alone (30 m

for TMT and 40 m for E-ELT), allowing the observation of more than 500 asteroids, even if we consider only objects that reach half (or 0.05″) of the current size limits (We computed the expected apparent diameter of asteroids for the 2020–2030 period, and counted objects when apparent diameters reach 0.05″ within this period.) Second-generation instruments with high-Strehl AO corrections into visible wavelengths are planned for these large ground-based telescopes, providing another factor of 5 improvement due to operation at shorter wavelengths. Together, these two factors should provide more than an order-of-magnitude improvement with respect to current resolution. Almost 7 000 asteroids should then be observable with apparent diameters greater than 0.01″. This breakthrough in imaging capabilities will also enable the spatial resolution of apparent disks of TNOs larger than 500 km, larger moons (∼100 km) of Uranus and Neptune, small moons of Jupiter and Saturn, main-belt asteroids of few tens of kilometers, and NEAs of several hundred meters in favorable conditions (Fig. 1).

2. Disk-resolved imaging observations

For asteroid (52) Europa, our primary data set was taken on 2005 January 20. In addition, we observed (52) Europa at one epoch on 2003 October 12, and at three epochs on 2007 May 28. In 2005 we obtained adaptive optics images of (52) Europa at H (1.6 μm) and Kp (2.1 μm) bands with NIRC2 (van Dam et al. 2004) on the Keck II 10 m telescope, and give the observing log in Table 1. The 2003 and 2005 images were taken using the first generation Keck wave-front controller; the 2007 images were taken using Keck's next generation wavefront controller (NGWFC, van Dam et al. 2007) under similar conditions. Strehl ratios were 30%, 27%, and 40% on average, respectively, for the 2003, 2005, and 2007 epochs. The latter, higher, value reflects the NGWFC changes which, in addition to a new detector, include improvements to the electronics and to the software. The data set consists of 111 images: 9 from 2003, 84 from 2005, and 18 from 2007, that result in 18 composite images (Table 1).

Although less extensive and at a larger distance from Earth, the 2007 data add an important new epoch to our 2005 data. By combining all 3 data sets (2003, 2005, and 2007), our goal was to derive a global fit that spans a wide range of viewing geometries and provide tight constraints on the size, shape, and pole for (52) Europa.

When observing at Kp in good seeing conditions, adaptive optics on Keck II delivers diffraction-limited resolution elements of width approximately 50 milli-arcsecond (mas). We used the narrow plate-scale (9.942 ± 0.050 mas/pixel) of the NIRC2 camera, oriented North-up (±0.15°, Konopacky et al. 2007) for all the observations.

3. Triaxial Ellipsoid (TE) Assumption

3.1. 2005 January 20

Each of seven sets of six H-band images and seven sets of six Kp-band images of asteroid (52) Europa obtained in 2005 was sky-subtracted, and then fit in the Fourier plane for the asteroid and Lorentzian PSF, using our method of Parametric Blind Deconvolution (PBD, as described by Drummond et al. 1998; Drummond 2000; Conrad et al. 2007). Asteroid ellipse parameters were computed as weighted means from each set of six images obtained at each filter and each rotational phase or epoch. These ellipse parameters (apparent major axis length α, minor axis length β, and an orientation angle PA_α), were then used to convert the series of apparent diameters and orientations to the full triaxial-ellipsoid diameters and direction of (52) Europa's rotational pole through a non-linear least squares inversion (see Drummond 2000, for instance). The results of the fit are given in Table 2.

In addition to the direct PBD methodology, as cross-checks, we use two additional avenues to get to the triaxial-ellipsoid solutions. In the first of these, the data were flat-fielded, shifted, and added at each rotational epoch (Fig. 2), and a single deconvolved image was created with the Mistral algorithm (Mugnier et al. 2004), for each epoch and each filter. These seven Kp and seven H deconvolved images (Fig. 3) were again fit in the Fourier plane for their apparent ellipse parameters, and the series was fit for the full triaxial solution, also given in Table 2.

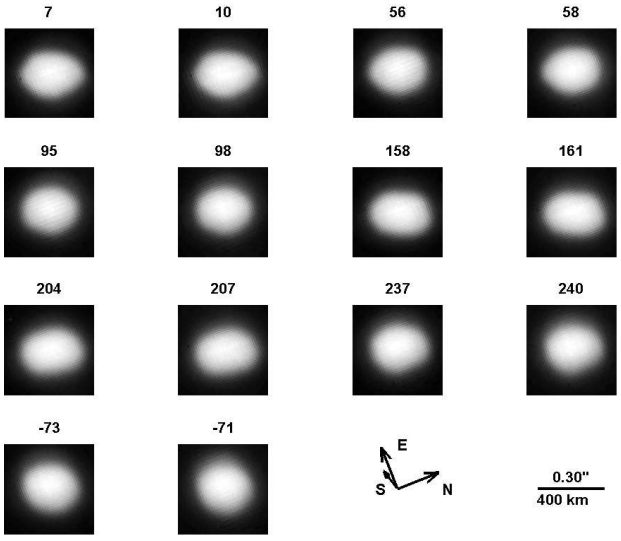


Figure 2: Sky-subtracted, flat-fielded, shifted, and added, images of (52) Europa, from 2005, before deconvolution, rotated so that the asteroid's spin axis is vertical. Although the direction to the Sun is indicated, the solar phase angle was only 5.5°, making the Sun nearly perpendicular to the plane of the figure. The rotational phase in degrees, ± 360°, of each tile is placed on top of it for placement in Fig 5. The Kp-band images are in the first and third columns while the H-band images always follow by a few degrees rotation in the second and fourth columns.

Finally, ellipse parameters were derived from fitting the edges produced by a Laplacian of Gaussian wavelet transform (Carry et al. 2008) on the Mistral deconvolved images. A full triaxial solution can then be found from these ellipse parameters, and is given in Table 2. The adopted triaxial solution for (52) Europa, independently determined from the 2005 data,

Date (UT)	Δ (AU)	r (AU)	ϕ (°)	m_V (mag)	φ (″)	Rotation phase (°)	Filter
2003-10-12 - 11:48	3.02	2.07	7.2	10.8	0.25	26	Kp
2005-01-20 - 10:39	2.79	1.84	5.5	10.3	0.28	6	Kp
2005-01-20 - 10:43	2.79	1.84	5.5	10.3	0.28	9	H
2005-01-20 - 11:25	2.79	1.84	5.5	10.3	0.28	55	Kp
2005-01-20 - 11:28	2.79	1.84	5.5	10.3	0.28	58	H
2005-01-20 - 12:02	2.79	1.84	5.5	10.3	0.28	95	Kp
2005-01-20 - 12:04	2.79	1.84	5.5	10.3	0.28	97	H
2005-01-20 - 13:01	2.79	1.84	5.5	10.3	0.28	157	Kp
2005-01-20 - 13:04	2.79	1.84	5.5	10.3	0.28	160	H
2005-01-20 - 13:45	2.79	1.84	5.5	10.3	0.28	204	Kp
2005-01-20 - 13:48	2.79	1.84	5.5	10.3	0.28	206	H
2005-01-20 - 14:16	2.79	1.84	5.5	10.3	0.28	237	Kp
2005-01-20 - 14:18	2.79	1.84	5.5	10.3	0.28	239	H
2005-01-20 - 15:02	2.79	1.84	5.5	10.3	0.28	-74	Kp
2005-01-20 - 15:05	2.79	1.84	5.5	10.3	0.28	-71	H
2007-05-28 - 11:44	3.41	2.69	13.3	11.9	0.19	105	Kp
2007-05-28 - 12:54	3.41	2.69	13.3	11.9	0.19	179	Kp
2007-05-28 - 13:01	3.41	2.69	13.3	11.9	0.19	186	Kp

Table 1: Observing log: heliocentric distance (Δ), range to observer (r), phase angle (ϕ), visual apparent magnitude (m_V), angular diameter (φ), and arbitrary rotation phase (zero phase being defined for a lightcurve maximum, *i.e.*, when the apparent cross-section of (52) Europa is the largest) for each epoch (reported in UT).

Parameter	PBD	Mistral	Edges	Mean
a (km)	377 ± 3	376 ± 3	381 ± 4	378 ± 3
b (km)	331 ± 3	332 ± 3	335 ± 4	332 ± 3
c (km)	236 ± 9	246 ± 8	249 ± 10	244 ± 8
SEP_β (°)	+27 ± 3	+25 ± 3	+25 ± 5	+25 ± 3
PA_{node} (°)	339 ± 1	339 ± 1	338 ± 1	338 ± 1
ψ_0 (UT)	10.35 ± 0.03	10.33 ± 0.03	10.28 ± 0.04	10.30 ± 0.03
EQJ2000 (α_0,δ_0 in °)	261;+10	260;+11	259;+12	260;+11
σ radius (°)	1	1	1	1
ECJ2000 (λ_0,β_0 in °)	260;+34	258;+34	257;+35	258;+34

Table 2: Triaxial-ellipsoid parameters for our 2005 data, with three different data-processing methods: PBD images, Mistral deconvolved images, and edge fitting. The average values for the parameters are reported in the last column. The quantities derived from the fits of the 2005 data are: triaxial ellipsoid diameters a, b, and c; the sub-Earth latitude SEP_β; the line of nodes (the intersection of the asteroid's equator and the plane of the sky) PA_{node}; and the UT of the instant when the long axis a lies in the plane of the sky along the line of nodes ψ_0. Uncertainties reported here are formal error bars of the fit, see the text for a discussion on the systematics.

is derived from the series of mean ellipse parameters at each epoch, that is, from the mean of the PBD images, the Mistral deconvolved images, and the edge-fitting at each epoch. This preferred mean fit is plotted against observations in Fig. 5. The location of the pole on the Ecliptic globe is shown in Fig. 6, along with the locations derived from lightcurves analysis by others.

Our imaging of (511) Davida (Conrad et al. 2007) showed large edge features that could be followed during rotation, even in the raw images. While there may be similar features on (52) Europa, they do not appear as consistently in the edge profiles and are not as easy to track. The features are not as large or prominent as those on Davida, relative to our reference ellipsoid. Later in the paper, we use 3-D shape modeling to try to study these departures from a pure ellipsoid shape.

3.2. 2007 May 28

We also acquired AO observations of (52) Europa at Keck in 2007 (Table 1). Following the recipe from the last section, we formed the mean apparent parameters from the three methods already described (PBD, deconvolved images, and outlines from the deconvolved images). Although not expected to yield significant results because the three 2007 observations provide only nine observables to find six unknowns, we nevertheless fit the three observations for a triaxial ellipsoid (Table 3 and Fig. 7), and found that the model is in surprisingly good agreement with the results from the 2005 set in Table 2.

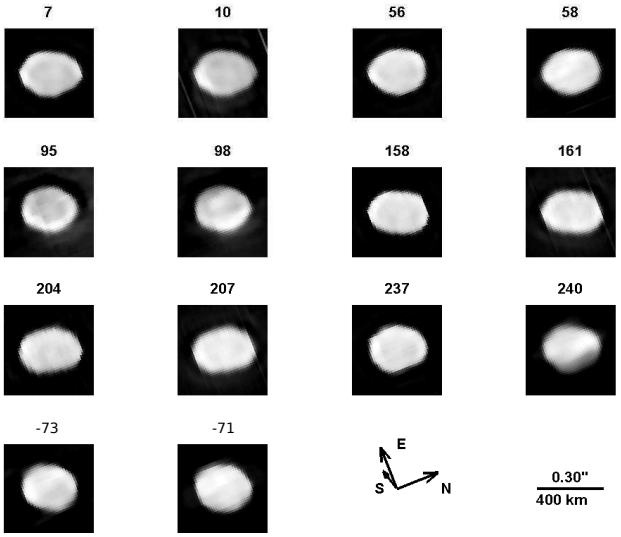


Figure 3: Same as in Fig. 2 for the MISTRAL deconvolved images of (52) Europa.

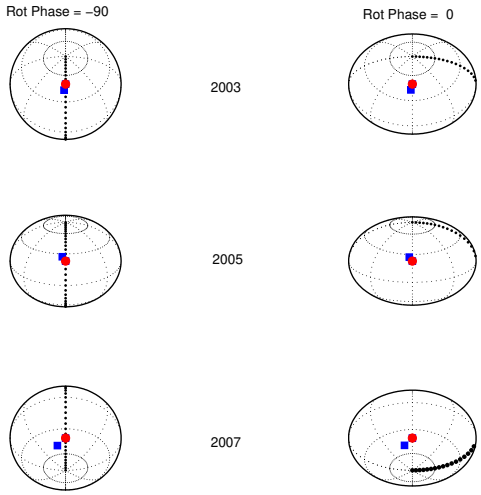


Figure 4: Plane-of-sky orientation of (52) Europa as seen during the 3 observing dates analyzed. The grids are in equatorial coordinates, with north up, east left. The blue square is the subsolar point and the red circle is the sub-Earth point. Two views for each are shown: the maximum (Rot Phase = 0) cross-section and the minimum (Rot Phase = -90) cross-section for that date. These phases are the same as those listed in the tables and Figs. 5, 7, and 8. The bold dotted line represents the line defined as longitude = 0, according to IAU convention (see Archinal et al. 2011). The longitude is related to the rotational phase by: longitude = 270° - Rot phase. The sense of rotation is given by the right-hand rule here, with the (positive) pole always northward, and can be discerned in the figure from the advancement of the bold dotted line by 90°.

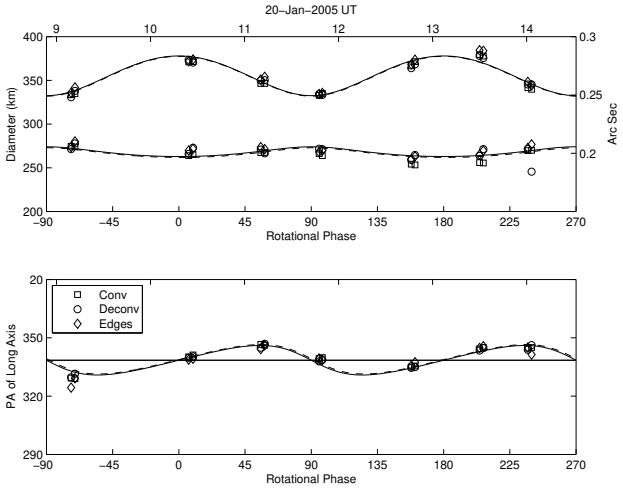


Figure 5: Triaxial ellipsoid fit to measured ellipse parameters for our 2005 data. In the upper subplot, each image's long and short axis dimensions are plotted along the upper and lower lines, respectively. The H-band epochs follow the Kp-band epochs by a few degrees, and the different symbols represent the different methods used to extract the ellipse parameters (PBD or Conv, MISTRAL or Deconv, and Edges). The solid lines are the prediction for the projected (full) ellipses from the mean triaxial ellipsoid parameters (Table 2). The dashed lines are for the ellipse parameters for the terminator ellipse, which, because the solar phase angle is only 5.5°, fall on the solid lines. The data should lie approximately midway between the dashed and solid lines (here, that means on the coincident solid/dashed lines). The lower subplot shows the position angle of the long axis (PA_α) with the same conventions.

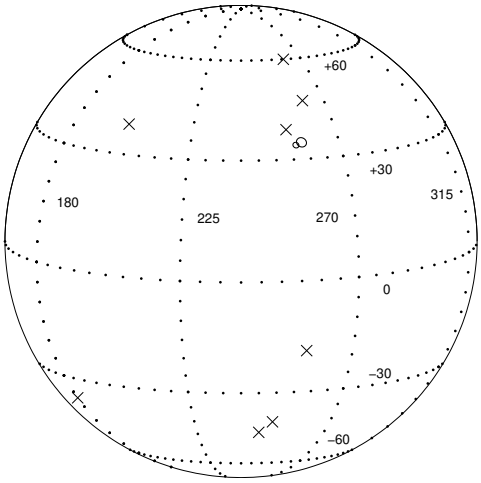


Figure 6: Pole locations for (52) Europa on the Ecliptic globe. The two circles denote the uncertainty areas around the pole found for 2005 (larger) and 2007 (smaller), while X's show the positions found from previous workers using lightcurves.

3.3. 2003 October 12

The single set of AO images of (52) Europa taken in 2003 (Table 1) does not allow an independent fit for a triaxial solution because it only provides three observables for six unknowns. We use these early Keck AO images, however, in a global fit in the next section. Fig. 8 shows the global fit prediction for the 2003 epoch, together with those data.

3.4. A global solution for all epochs

We can tie the 2003, 2005, and 2007 observations of (52) Europa together into one simultaneous global fit (Drummond et al., 2012, in preparation), using the sidereal period of $P_s = 0.2345816$ days (with an uncertainty of 2 in the last digit) derived by Michałowski et al. (2004). Along with the global solution for the triaxial dimensions and pole in Table 4, we list

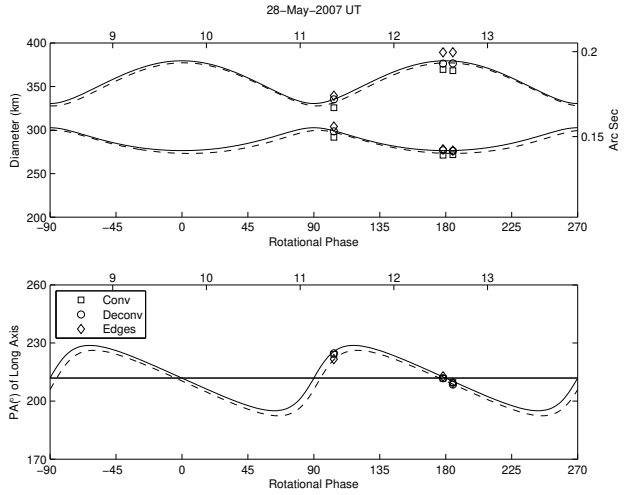


Figure 7: Same as Fig. 5, but for 2007. The maximum that occurs at 9.74±0.01, lighttime corrected, is the same hemisphere as the maximum that occurs at 10.30 UT in Fig. 5.

Parameter	Mean
a (km)	379 ± 1
b (km)	330 ± 1
c (km)	225 ± 9
SEP_β (°)	-41 ± 5
PA_{node} (°)	212 ± 1
ψ_0 (UT)	9.74 ± 0.01
EQJ2000 (α_0,δ_0 in °)	258;+11
σ radius (°)	1
ECJ2000 (λ_0,β_0 in °)	256;+34

Table 3: Triaxial Ellipsoid Fit Parameters from 2007 observations. Uncertainties reported here are formal error bars of the fit, see the text for a discussion on the systematics.

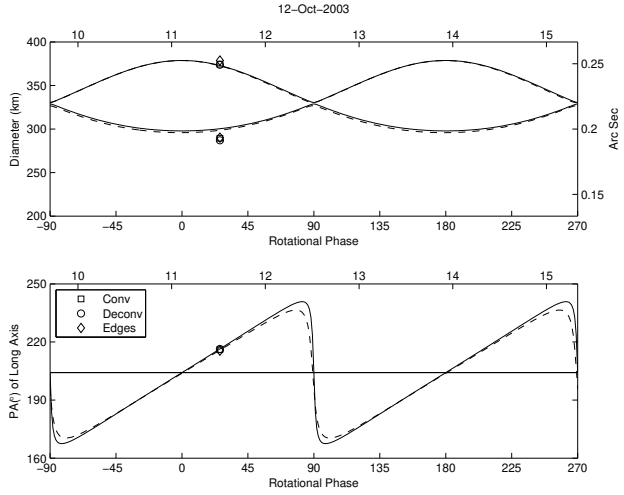


Figure 8: Global fit and 2003 data.

the three parameters that differ due to the changing angles for each date.

Statistical uncertainties for the dimensional parameters, as well as those involving angles, such as pole position and longitude of the node, come from the non-linear least-squares fit for the 6 parameters that define the TE model, the 3 diameters and 3 Euler angles. Systematic effects can arise in the process of constructing a 3-D description of an asteroid from information limited to a 2-D plane (images). Therefore, one needs to be particularly vigilant regarding model assumptions, and their appropriateness for a particular situation. While the uncertainties derived for the parameters as fit by the model are straightforward, estimating the systematic effects that are present is not. Deriving realistic (and therefore, directly applicable by other workers) uncertainties for our results, including possible systematics, is the most challenging aspect of our work.

We have carefully calibrated some of these uncertainties by making observations of external sources (*e.g.*, the moons of Saturn) of known size. One of the results of that work has shown that our systematic uncertainties are larger for objects of smaller angular diameter, until we reach a limit (at about 0.09″for a 10 m telescope) where we can no longer get reliable sizes. Aspect ratios of projected shapes are still possible, but absolute sizes break down. We have found that our systematics from these tests span about 1–4% per linear dimension. In addition, we have also imaged targets of spacecraft missions prior to flyby (see KOALA section). In the case of (21) Lutetia, despite an angular size of only 0.10″, our resulting models were good to 2% in size and 2 km RMS in topography on a 100 km object (see Carry et al. 2012).

We can also compare our TE results with those of KOALA (see below), in cases where we have adequate observations. In particular, we have such comparisons for four asteroids, including (52) Europa. We can look for consistency, not only between the two techniques, but in sub-sets of data to learn how far we fall from the "correct" values. We can also compare the results of data sets from different years. Our upcoming article, mentioned above (Drummond et al., in preparation) will be a standalone treatment of the global fitting technique and calibration that will include much detail on uncertainties. For the present results, we have determined that we should add quadratically systematic uncertainties of 4.1%, 2.3%, and 3.8% to the TE-derived fit errors (given in Table 4) for a, b, c, respectively. The resulting total uncertainty estimates for the a, b, c diameters are $16 \times 8 \times 10$ km, with a 7 degree systematic uncertainty for the orientation of the spin axis. See Fig. 4 for a visualization of the orientation of (52) Europa on the plane of the sky.

4. Comparison of (52) Europa to Lightcurves Inversion Model

From optical lightcurves of (52) Europa, Michałowski et al. (2004) found a rotational pole at [λ_0, β_0]=[252°, +38°], with a 5° uncertainty in each Ecliptic coordinate. It is the pole closest to ours in Fig. 6, about 6° away. They derived an a/b axial ratio of 1.15, the same as our 1.15 ± 0.04, and a b/c ratio of 1.3, compared with our 1.33 ± 0.05.

Diameter (km)	Pole	Param	2003 Oct 12	2005 Jan 20	2007 May 28
a = 379 ± 2	(α_0,δ_0) = 257°;+12°	SEP_β (°)	+49 ± 1	+23 ± 1	-40 ± 1
b = 330 ± 2	σ radius = 1°	PA_{node} (°)	204 ± 1	339 ± 1	213 ± 1
c = 249 ± 3	(λ_0,β_0) = 255°;+35°	ψ_0 (UT)	11.11 ± 0.02	10.31 ± 0.02	9.72 ± 0.02

Table 4: Results for the global fit. Uncertainties reported here are formal error bars of the fit. Including systematic effects raises the total uncertainties to $16\times8\times10$ km for the three ellipsoid diameters, and to 7° in the pole.

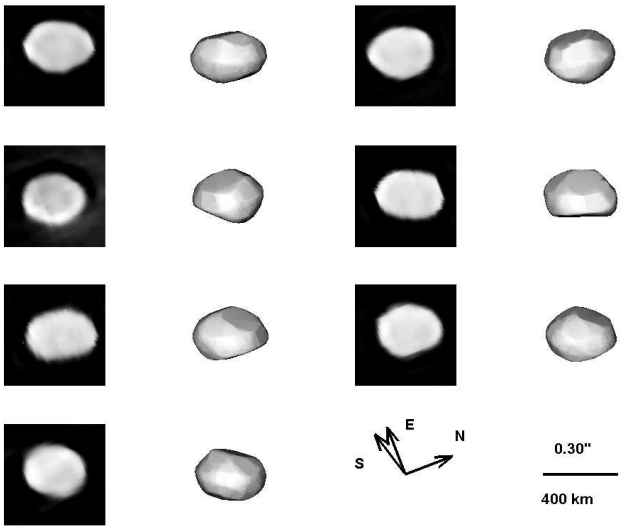


Figure 9: Comparison of our (2005) deconvolved K images from Fig. 3 (columns 1 and 3) with the web model of Michałowski et al. (2004), projected forward from 1983 using their sidereal period of 0.2345816 days and an update (although nearly identical) to thier pole from DAMIT (columns 2 and 4).

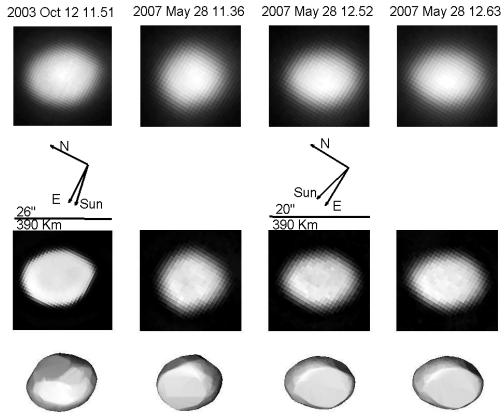


Figure 10: Same as Fig. 9, but for 2003 and 2007. In addition to the deconvolved images in the middle row, we show the non-deconvoled, shifted, and centered images in the top row for each epoch. In 2003, (52) Europa was 1.3 times closer than in 2007 resulting in different scales for the two years.

Figure 9 is a side by side comparison of our deconvolved Kp images, from 2005 January 20 (from Fig. 3) and the Michałowski et al. model, using the updated rotational pole for the model at $[\lambda_0, \beta_0]$=[251°; +35°] from the DAMIT (Ďurech et al. 2010) web site[1]. Figure 10 shows comparison between our convolved and deconvolved images and the lightcurves inversion model for 2003 and 2007.

The overall agreement between our AO deconvolved images and the model predictions is excellent. A careful examination of Figs 9 and 10, however, will show edge features that are seen in one but not the other, requiring the development of an updated shape model, as discussed in following section. Despite these features, (52) Europa is still well-modeled as a smooth triaxial ellipsoid.

5. KOALA 3-D shape model

We construct a 3-D shape model of (52) Europa to give a better rendering of the apparent shape visible in the images. For that, we use our KOALA algorithm (Carry et al. 2010a; Kaasalainen 2011) that makes combined use of optical lightcurves, stellar occultations timings, and profiles from disk-resolved images. The results of KOALA have been recently validated at (21) Lutetia by the images taken by the ESA Rosetta mission: The 3-D shape model and spin orientation determined before the encounter by combining AO images and lightcurves (Carry et al. 2010b) were in complete agreement with images and results from the flyby (Sierks et al. 2011; Carry et al. 2012). Axial dimensions from KOALA were determined within 2% of the the actual values and RMS differences in topography were only 2 km.

We use here the 18 imaging epochs described in Sect. 2, together with 49 lightcurves taken between 1979 and 2011 (we acquired 8 additional lightcurves within the CdR/CdL collaboration with respect to the 41 lightcurves presented by Michałowski et al. 2004), and 4 stellar occultations (timings taken from Dunham et al. 2011). A comparison of the KOALA 3-D shape model with the AO images from 2005 is presented in Fig. 11. The agreement between the 3-D shape model and the data is very good. The typical deviation with the 18 imaging contours is of 0.2 pixel, corresponding to a few km. The 49 lightcurves are rendered at a level of 0.03 mag, *i.e.*, close to the intrinsic level of uncertainty of the data. Finally, the residuals between the occultation chords and the model are 13 km, on average, mainly owing to the lower quality of 1983 occultation timings (residuals of 19 km, compared to 11, 13, and 6 km for the other epochs). Figure 12 shows these chords mapped onto

[1] http://astro.troja.mff.cuni.cz/projects/asteroids3D/web.php

the projections of the 3-D KOALA model for the epochs of the occultations.

The 3-D shape derived with KOALA is close to an ellipsoid, validating (52) Europa as a Standard Triaxial Ellipsoid Asteroid (STEA, Drummond et al. 2008). Fitting the KOALA model as a triaxial ellipsoid yields diameters of $368 \times 327 \times 255$ km, in excellent agreement with the diameters and total uncertainties in Table 4. The volume-equivalent spherical-diameter of the KOALA 3-D shape model, derived by summing volume cells, is 312 ± 6 km, in excellent agreement with the TE analysis presented above. The KOALA model yields a spin pole within 3° of $[\lambda_0, \beta_0]$=[254°; +37°] or $[\alpha_0, \delta_0]$=[257°; +15°], also close to the TE result. The shape model can be downloaded from the DAMIT web page.

6. Occurrence of large facets on C-type asteroids

The 3-D shape model presents two broad shallow depressions, probably best noted in the lower right of Fig. 12. They can also be seen on the tops and bottoms of the asteroid images in column 1, panel 3, and column 3, panel 2. The departures from an ellipsoid, however, are not nearly as significant as the apparent giant facets seen in our analysis of (511) Davida (Conrad et al. 2007), nor as prominent, relative to body size, as the giant craters seen on (253) Mathilde (Veverka et al. 1997). We chose Mathilde as a prototypical object displaying giant features seen in profile (craters/facets), although Mathilde was a much smaller asteroid than Davida. But it turns out that (52) Europa is almost a twin of Davida in many respects: both are C-type asteroids of very nearly the same size, they have similar spin periods, and they have similar orbital properties, so they have likely seen the same impact environment (although Davida does have a bit larger eccentricity and inclination). In the Davida paper, we went to some length to demonstrate that Davida could have encountered impacts of the size necessary to produce the giant facets seen, without having broken up the body. So given the similarities between Davida and (52) Europa, one might now wonder how likely it is that (52) Europa would *not* show such facets (or at least not show facets that are quite as prominent).

Returning to our analysis in the Davida paper, we estimated that Davida should have had about 2.5 impacts large enough to make such a giant crater during its lifetime. This led to the conclusion that if the facets seen were indeed craters, seen edge-on, as on Mathilde, they would not be unexpected. The same statistics should hold true for (52) Europa. But with an expected total of only 2.5 impacts of this size during its lifetime, the chances are also reasonable that it did not encounter any such impacts. We therefore conclude that *not seeing* such prominent features on a twin such as (52) Europa could also be expected. Of course, the flux of smaller impactors would be higher, and these would be responsible for the perhaps less prominent edge features that we do see. Given that the viewing geometry has to be just right to see these types of facets, it is possible that observational circumstances have conspired such that we missed some giant feature, or such that those facets we do see are less pronounced or are particularly hard to follow with rotation. We have a fairly wide range of latitudes and longitudes in our data set, however, so the chances of missing something as prominent as a Davida-style facet are diminished, and we assert that Europa appears qualitatively different than Davida.

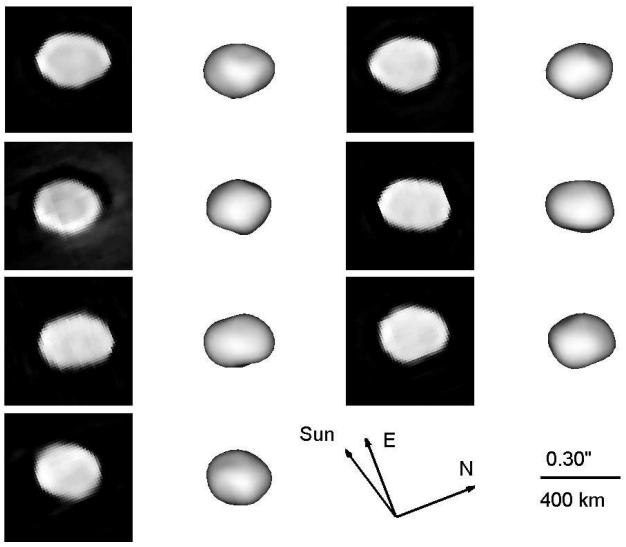


Figure 11: Comparison of our 2005 deconvolved Kp images from Fig. 3 (columns 1 and 3) with the KOALA model described here

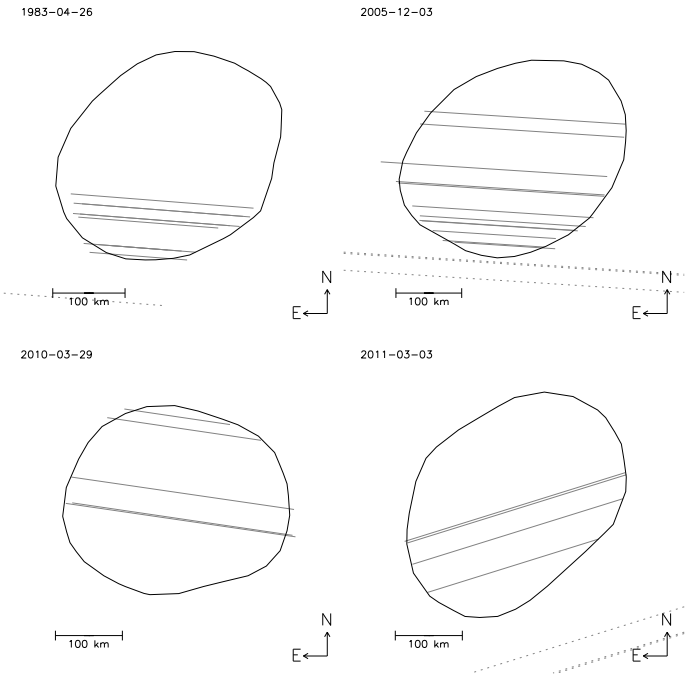


Figure 12: Comparison of the four stellar occultations with the KOALA shape model. Solid and dashed grey lines represent positive (hits) and negative (misses) chords, respectively. Black contours are the projection of the KOALA 3-D shape model on the plane of the sky at each occultation epoch.

7. Density of (52) Europa

There are 17 estimates of the mass of (52) Europa available in the literature, derived either from the analysis of the orbit's deflection during close approaches of minor planets to (52) Europa (*e.g.*, Michalak 2001), or from a general adjustment of the parameters used to generate the ephemeris of the planets and asteroids in the Solar System (*e.g.*, Fienga et al. 2009). We adopt here the weighted mean of these determinations (following the selection discussed in Carry 2012): $(2.38 \pm 0.58) \times 10^{19}$ kg.

In general, the differences in volume between the triaxial and the KOALA models are small. Here, that difference is less than 1%, which would lead to a volume difference of less than 3%. When assigning uncertainties to our sizes (from either method), we not only assess the derivable statistical uncertainties, but we must also provide an estimate of systematic effects, of which this difference is an example. The uncertainties used already include potential differences between the models. Because of the added topographic detail provided by the KOALA model, we choose, in this case, to use the KOALA-derived volume of $(1.59 \pm 0.10) \times 10^7$ km^3, giving a density of 1.5 ± 0.4 g cm^{-3}. This bulk density falls within the observed range of densities for C-type asteroids. Here, the uncertainty is mainly due to the uncertainty on the mass determination (24%) rather than the volume uncertainty of 6%. Thus, we are at the point in the study of the density of asteroids where the uncertainty on the volume is no longer the limiting factor (volume determination remains generally the limiting factor when the mass is estimated from a spacecraft encounter or a satellite, see the review by Carry 2012).

Dedicated observing programs and theoretical work are now needed to derive more accurate masses of large main-belt asteroids. The advent of the Gaia mission (expected launch 2013) should contribute a large number of new, improved masses (see Mouret et al. 2007, for instance). With these more reliable volumes and masses, we can derive improved densities and porosities, which in turn will allow us to better understand how density and porosity may be related to taxonomic class, absolute diameters, or location (*e.g.*, inner vs. outer main belt). And this highlights the importance of continuing to push for more AO observations of asteroids for size/shape determination, from the best facilities, and the continued development of techniques, such as KOALA, that combine multiple data types (hopefully, eventually to include thermal radiometry and radar echoes).

8. Summary

At this point, (52) Europa can be considered for membership as a Standard Triaxial Ellipsoid Asteroid (STEAs, see Drummond et al. 2008) because it is so well modeled as an ellipsoid (like asteroid (511) Davida, see Conrad et al. 2007). The ellipses projected by these standard ellipsoids can be predicted well into the future or past, and therefore, can be used as calibration objects for other techniques used in studying asteroids. Conrad et al. (2007) and Drummond et al. (in preparation) detail the equations necessary to predict the asterocentric latitudes and longitudes, and Drummond (2000) show how to derive the projected ellipse parameters from the asterocentric latitudes and longitudes. For example, (52) Europa's asterocentric latitude can be predicted to within the error of its rotational pole, 7°, and its asterocentric longitude to within 0.5°/yr since the date of the most recent epoch reported here (2007 May 28). The longitude uncertainty arises from the formal uncertainty in the sidereal period, but in fact, judging by the good agreement shown between the images and lightcurves inversion model projected forward from 1983, longitudes should be predictable to a much higher accuracy than these values indicate. The projected major or minor axis dimensions can be predicted to within approximately the uncertainty found here of 5–10 km, and the orientation of the apparent ellipse to within 2°.

We are fortunate to have both the triaxial ellipsoid (TE, Drummond et al. 2009a) and the KOALA (Carry et al. 2010a) techniques available for our analysis of AO images of asteroids. Each has its own strengths. TE requires relatively few images, can return shape/size/pole information amazingly quickly, is generally insenstive to changes in the PSF, and is usually adequate to get the basic asteroid parameters. For more detailed 3-D shape information we can rely on KOALA. Unlike lightcurve inversion alone, KOALA can obtain absolute sizes, and is sensitive to concavities. The methods can be used to validate each other, as we found exceedingly useful during our analysis of the Lutetia data, prior to the Rosetta flyby (Drummond et al. 2010; Carry et al. 2010b). And while a detailed 3-D shape model might be seen to supercede the triaxial assumption of TE, that is not necessarily the case. As an example, our AO imaging of the close flyby of Near-Earth Asteroid 2005 YU55 from Keck, in November 2011, resulted in almost immediate size and shape information from TE (Merline et al. 2011). In futher analysis, we had hoped to use numerous lightcurves, taken near the time of the flyby, to help refine the size/shape with KOALA. But despite our efforts, the lightcurve information on 2005 YU55 so-far is insufficient (mostly due to a very slow spin period) to allow KOALA to improve significantly on TE. This demonstrates the importance of having both methods available for analysis of our asteroid data.

New imaging, lightcurve, and occultation data will be added to our overall analysis for (52) Europa as they become available. These may allow us to distinguish whether any of the somewhat-flattened edges seen on (52) Europa in our existing data sets are indeed facets or craters of the type seen on Davida and Mathilde, and to better evaluate the extent and morphology of any departure from a pure ellipsoid. The techniques we are developing here (both observational and in data analysis) will allow us to make immediate and substantial advances once data from new, larger telescopes can be acquired.

Acknowledgments

This work presented here was supported by grants from NASA's Planetary Astronomy Program and the U.S. National Science Foundation, Planetary Astronomy Program. We are grateful for telescope time made available to us by the NASA TAC, and also for the support of our collaborators on Team

Keck, the Keck science staff. The work of J. Ď was supported by grant P209/10/0537 of the Czech Science Foundation and by the Research Program MSM0021620860 of the Ministry of Education.

This research has made use of NASA's Astrophysics Data System. The authors wish to recognize and acknowledge the very significant cultural role and reverence that the summit of Mauna Kea has always had within the indigenous Hawaiian community. We are most fortunate to have the opportunity to conduct observations from this mountain.

References

B. A. Archinal, M. F. A'Hearn, E. Bowell, A. Conrad, G. J. Consolmagno, R. Courtin, T. Fukushima, D. Hestroffer, J. L. Hilton, G. A. Krasinsky, G. Neumann, J. Oberst, P. K. Seidelmann, P. Stooke, D. J. Tholen, P. C. Thomas, and I. P. Williams, 2011. Report of the IAU Working Group on Cartographic Coordinates and Rotational Elements: 2009. Celestial Mechanics and Dynamical Astronomy, 109:101–135.

D. T. Britt, G. J. Consolmagno, and W. J. Merline. Small Body Density and Porosity: New Data, New Insights. In S. Mackwell & E. Stansbery, editor, 37th Annual Lunar and Planetary Science Conference, volume 37 of Lunar and Planetary Inst. Technical Report, page 2214, 2006.

D. T. Britt, D. K. Yeomans, K. R. Housen, and G. J. Consolmagno, 2002. Asteroid Density, Porosity, and Structure. Asteroids III, pages 485–500.

B. Carry. Asteroids physical properties from high angular-resolution imaging. PhD thesis, Observatoire de Paris, 2009.

B. Carry, 2012. Density of asteroids. Planetary and Space Science, 73:98–118.

B. Carry, C. Dumas, M. Fulchignoni, W. J. Merline, J. Berthier, D. Hestroffer, T. Fusco, and P. Tamblyn, 2008. Near-Infrared Mapping and Physical Properties of the Dwarf-Planet Ceres. Astronomy and Astrophysics, 478(4): 235–244.

B. Carry, C. Dumas, M. Kaasalainen, J. Berthier, W. J. Merline, S. Erard, A. R. Conrad, J. D. Drummond, D. Hestroffer, M. Fulchignoni, and T. Fusco, 2010a. Physical properties of (2) Pallas. Icarus, 205:460–472.

B. Carry, M. Kaasalainen, C. Leyrat, W. J. Merline, J. D. Drummond, A. R. Conrad, H. A. Weaver, P. M. Tamblyn, C. R. Chapman, C. Dumas, F. Colas, J. C. Christou, E. Dotto, D. Perna, S. Fornasier, L. Bernasconi, R. Behrend, F. Vachier, A. Kryszczynska, M. Polinska, M. Fulchignoni, R. Roy, R. Naves, R. Poncy, and P. Wiggins, 2010b. Physical properties of the ESA Rosetta target asteroid (21) Lutetia. II. Shape and flyby geometry. Astronomy and Astrophysics, 523:A94.

B. Carry, M. Kaasalainen, W. J. Merline, T. G. Müller, L. Jorda, J. D. Drummond, J. Berthier, L. O'Rourke, J. Ďurech, M. Küppers, A. R. Conrad, C. Dumas, H. Sierks, and the OSIRIS TeamPSS, 2012. KOALA shape modeling technique validated at (21) Lutetia by ESA Rosetta mission. Planetary and Space Science, 66:200–212.

A. R. Conrad, C. Dumas, W. J. Merline, J. D. Drummond, R. D. Campbell, R. W. Goodrich, D. Le Mignant, F. H. Chaffee, T. Fusco, S. H. Kwok, and R. I. Knight, 2007. Direct measurement of the size, shape, and pole of 511 Davida with Keck AO in a single night. Icarus, 191(2):616–627.

J. D. Drummond. Measuring Asteroids with Adaptive Optics. In N. Ageorges and C. Dainty, editors, Laser Guide Star Adaptive Optics for Astronomy, pages 243–262, 2000.

J. D. Drummond, J. C. Christou, and J. Nelson, 2009a. Triaxial ellipsoid dimensions and poles of asteroids from AO observations at the Keck-II telescope. Icarus, 202:147–159.

J. D. Drummond, A. Conrad, W. Merline, and B. Carry, 2009b. The Dimensions and Pole of Asteroid (21) Lutetia from Adaptive Optics Images. AAS/Division for Planetary Sciences Meeting Abstracts, 41:# 59.07.

J. D. Drummond, A. Conrad, W. J. Merline, B. Carry, C. R. Chapman, H. A. Weaver, P. M. Tamblyn, J. C. Christou, and C. Dumas, 2010. Physical properties of the ESA Rosetta target asteroid (21) Lutetia. I. The triaxial ellipsoid dimensions, rotational pole, and bulk density. Astronomy and Astrophysics, 523:A93.

J. D. Drummond, R. Q. Fugate, J. C. Christou, and E. K. Hege, 1998. Full Adaptive Optics Images of Asteroids Ceres and Vesta; Rotational Poles and Triaxial Ellipsoid Dimensions. Icarus, 132:80–99.

J. D. Drummond, W. J. Merline, A. Conrad, C. Dumas, and B. Carry. Standard Triaxial Ellipsoid Asteroids from AO Observations. In AAS/Division for Planetary Sciences Meeting Abstracts #40, volume 40 of Bulletin of the American Astronomical Society, page 427, 2008.

D. W. Dunham, D. Herald, E. Frappa, T. Hayamizu, J. Talbot, and B. Timerson. Asteroid Occultations. NASA Planetary Data System, 2011. EAR-A-3-RDR-OCCULTATIONS-V9.0.

J. Ďurech, V. Sidorin, and M. Kaasalainen, 2010. DAMIT: a database of asteroid models. Astronomy and Astrophysics, 513:A46.

A. Fienga, J. Laskar, T. Morley, H. Manche, P. Kuchynka, C. Le Poncin-Lafitte, F. Budnik, M. Gastineau, and L. Somenzi, 2009. INPOP08, a 4-D planetary ephemeris: from asteroid and time-scale computations to ESA Mars Express and Venus Express contributions. Astronomy and Astrophysics, 507:1675–1686.

M. Kaasalainen, 2011. Maximum compatibility estimates and shape reconstruction with boundary curves and volumes of generalized projections. Inverse Problems and Imaging, 5(1):37–57.

Q. M. Konopacky, A. M. Ghez, G. Duchêne, C. McCabe, and B. A. Macintosh, 2007. Measuring the Mass of a Pre-Main-Sequence Binary Star through the Orbit of TWA 5A. Astronomical Journal, 133:2008–2014.

W. J. Merline, J. D. Drummond, P. M. Tamblyn, B. Carry, C. Neyman, A. R. Conrad, C. R. Chapman, J. C. Christou, C. Dumas, and B. L. Enke, 2011. 2005 YU_55. IAU Circular, 9242:1.

W. J. Merline, J. D. Drummond, P. M. Tamblyn, B. Carry, C. Neyman, A. R. Conrad, C. R. Chapman, J. C. Christou, C. Dumas, and B. L. Enke. Keck Adaptive-Optics Imaging of Near-Earth Asteroid 2005_YU55 during its 2011 Close Flyby. In Asteroids, Comets, Meteors Meeting, Japan, number 6372, 2012.

W. J. Merline, S. J. Weidenschilling, D. D. Durda, J.-L. Margot, P. Pravec, and A. D. Storrs, 2002. Asteroids Do Have Satellites. Asteroids III, pages 289–312.

G. Michalak, 2001. Determination of asteroid masses. II. (6) Hebe, (10) Hygiea, (15) Eunomia, (52) Europa, (88) Thisbe, (444) Typtis, (511) Davida and (704) Interamnia. Astronomy and Astrophysics, 374:703–711.

T. Michałowski, T. Kwiatkowski, M. Kaasalainen, W. Pych, A. Kryszczyńska, P. A. Dybczyński, F. P. Velichko, A. Erikson, P. Denchev, S. Fauvaud, and G. M. Szabó, 2004. Photometry and models of selected main belt asteroids I. 52 Europa, 115 Thyra, and 382 Dodona. Astronomy and Astrophysics, 416: 353–366.

S. Mouret, D. Hestroffer, and F. Mignard, 2007. Asteroid masses and improvement with GAIA. Astronomy and Astrophysics, 472:1017–1027.

L. M. Mugnier, T. Fusco, and J.-M. Conan, 2004. MISTRAL: a Myopic Edge-Preserving Image Restoration Method, with Application to Astronomical Adaptive-Optics-Corrected Long-Exposure Images. Journal of the Optical Society of America A, 21(10):1841–1854.

D. Nesvorný, W. F. Bottke, Jr., L. Dones, and H. F. Levison, 2002. The recent breakup of an asteroid in the main-belt region. Nature, 417:720–771.

H. Sierks, P. Lamy, C. Barbieri, D. Koschny, H. Rickman, R. Rodrigo, M. F. A'Hearn, F. Angrilli, A. Barucci, J.-L. Bertaux, I. Bertini, S. Besse, B. Carry, G. Cremonese, V. Da Deppo, B. Davidsson, S. Debei, M. De Cecco, J. De Leon, F. Ferri, S. Fornasier, M. Fulle, S. F. Hviid, G. W. Gaskell, O. Groussin, P. J. Gutierrez, L. Jorda, M. Kaasalainen, H. U. Keller, J. Knollenberg, J. R. Kramm, E. Kührt, M. Küppers, L. M. Lara, M. Lazzarin, C. Leyrat, J. L. Lopez Moreno, S. Magrin, S. Marchi, F. Marzari, M. Massironi, H. Michalik, R. Moissl, G. Naletto, F. Preusker, L. Sabau, W. Sabolo, F. Scholten, C. Snodgrass, N. Thomas, C. Tubiana, P. Vernazza, J.-B. Vincent, K.-P. Wenzel, T. Andert, M. Pätzold, and B. P. Weiss, 2011. Images of asteroid (21) Lutetia: A remnant planetesimal from the early Solar System. Science, 334:487–490.

P. C. Thomas, R. P. Binzel, M. J. Gaffey, A. D. Storrs, E. N. Wells, and B. H. Zellner, 1997. Impact excavation on asteroid 4 Vesta: Hubble Space Telescope results. Science, 277:1492–1495.

M. A. van Dam, E. M. Johansson, P. J. Stomski Jr., R. Sumner, J. C. Y. Chin, and P. L. Wizinowich. Performance of the Keck II AO system, 2007.

M. A. van Dam, D. Le Mignant, and B. Macintosh, 2004. Performance of the Keck Observatory adaptive-optics system. Applied Optics, 43(23):5458–5467.

J. Veverka, P. C. Thomas, A. Harch, B. E. Clark, J. F. Bell, B. Carcich, J. Joseph, C. R. Chapman, W. J. Merline, M. S. Robinson, M. Malin, L. A. McFadden, S. L. Murchie, S. E. Hawkins, R. Faquhar, N. Izenberg, and A. F. Cheng, 1997. NEARs Flyby of 253 Mathilde: Images of a C Asteroid. Science,

278:2109–2114.

J. Veverka, P. C. Thomas, A. Harch, B. E. Clark, B. Carcich, J. Joseph, S. L. Murchie, N. Izenberg, C. R. Chapman, W. J. Merline, M. Malin, L. A. McFadden, and M. S. Robinson, 1999. NEAR Encounter with Asteroid 253 Mathilde: Overview. Icarus, 140:3–16.